Area-Independence of the Biexciton Oscillator Strength in CdSe Colloidal Nanoplatelets

Carmelita Rodà,[†,‡] Pieter Geiregat,[†,‡] Alessio Di Giacomo,[†,‡] Iwan Moreels,[†,‡] and Zeger Hens[*,†,‡]

†*Physics and Chemistry of Nanostructures, Department of Chemistry, Ghent University, 9000 Gent, Belgium*

‡*NB-Photonics - Center for Nano- and Biophotonics, Ghent University, 9000 Gent, Belgium*

E-mail: zeger.hens@ugent.be

Abstract

Colloidal CdSe nanoplatelets (NPLs) are unique systems to study two-dimensional excitons and excitonic complexes. However, while absorption and emission of photons through exciton formation and recombination has been extensively quantified, little studies have addressed the exciton-biexciton transition. Here, we use cross-polarized pump-probe spectroscopy to measure the absorption coefficient spectrum of this transition and determine the biexciton oscillator strength (f_{BX}). We show that f_{BX} is independent of the NPL area, and that the concomitant biexciton area (S_{BX}) agrees with predictions of a short-range interaction model. Moreover, we show that f_{BX} is comparable to the oscillator strength of forming localized excitons at room temperature, while being unaffected itself by center-of-mass localization. These results confirm the relevance of biexcitons for light-matter interaction in NPLs. Moreover, the quantification of the exciton-biexcition transition introduced here will enable researchers to

rank 2D materials by the strength of this transition, and compare experimental results with theoretical predictions.

Keywords

2D Materials, Excitons, Optical Properties, Pump-Probe Spectroscopy

Two-dimensional colloidal semiconductor nanocrystals – nanoplatelets (NPLs) in brief – offer unique opportunities to investigate excitons (X) in quantum wells at room temperature.[1–3] Considering the seminal example of CdSe NPLs, dielectric confinement enhances the electron-hole Coulomb interaction and makes the exciton binding energy exceed thermal energy at room temperature by about one order of magnitude.[4–8] Concomitantly, the absorbance spectra of these NPLs exhibit pronounced exciton lines.[9] Given these features, light absorption to form excitons and radiative recombination by excitons have been interpreted in terms of a giant exciton oscillator strength $f_{\mathrm{X},tot}$, a wording referring to the amplification of the exciton oscillator strength caused by the delocalization of the exciton center-of-mass over the entire NPL area S_{NPL},[10–12] see Figure 1a. Furthermore, the possibility to form at room temperature stable excitonic complexes, such as biexcitons (BX) — a bound state of two excitons — has been linked to the low threshold to reach population inversion by optical pumping in NPLs, and the considerable material gain NPLs can provide.[13–19] Interestingly, in the case of epitaxially grown quantum wells, light-matter interaction through biexciton formation has been equally discussed in terms of a giant oscillator strength.[20] For the exciton-to-biexciton (X $\rightarrow$ BX), however, this oscillator strength magnification is re-

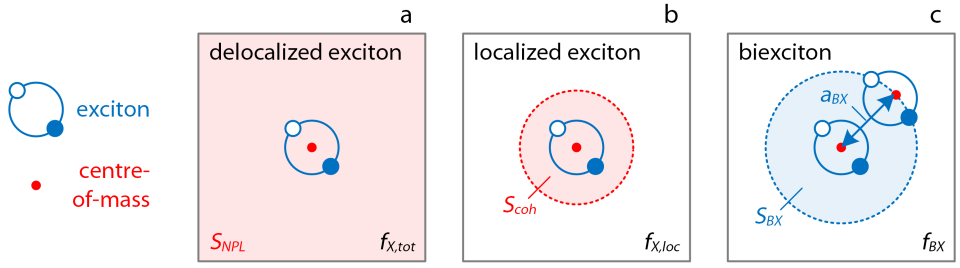

Figure 1: Representation of excitons and excitonic complexes in nanoplatelets (NPLs). (a) Delocalized exciton as a bound state of an electron and a hole; the delocalization of the center-of-mass across the entire NPL, as represented by the red shaded area, leads to a giant oscillator strength $f_{\mathrm{X},tot}$ that scales with the NPL area S_{NPL}. (b) Localized exciton as a bound state of an electron and a hole; the localization of the center-of-mass into the coherence area S_{coh} yields a reduced oscillator strength $f_{\mathrm{X},loc}$ independent of the NPL area. (c) The biexciton as a bound state of two excitons; the biexciton radius a_{BX} defines a biexciton area, represented by the blue shaded area; the concomitant biexciton oscillator strength f_{BX} is expected to be independent of the NPL area.

lated to the biexciton area S_{BX} rather than the NPL area, where S_{BX} is the area covered by the internal coordinate a_{BX} measuring the average exciton-exciton interdistance,[21] see Figure 1c. In the case of colloidal NPLs, a similar reasoning was applied previously to compare the radiative rate of exciton and trion emission at cryogenic temperatures, which scaled in proportion to the NPL area and the trion Bohr radius, respectively.[22]

Recently, optical Stark measurements were used to show that light-matter interaction through excitons at room temperature in CdSe NPLs is best understood by considering excitons as bound electron-hole pairs with a center-of-mass localized within the exciton coherence area S_{coh} rather than the total NPL area.[12,23] Exciton localization can be brought about by lattice faults or lattice vibrations, and, as outlined in Figure 1b, breaks down the giant exciton oscillator strength $f_{\mathrm{X},tot}$ into multiple smaller contributions $f_{\mathrm{X},loc}$ from localized excitons. This localized oscillator strength is diminished relative to $f_{\mathrm{X},tot}$ by the ratio S_{coh}/S_{NPL}.[12,24] With a coherence area estimated at $\sim 6\,\mathrm{nm}^2$ for 4.5 monolayer (ML) thick NPLs, localization can easily reduce the exciton oscillator strength by 1 to 2 orders of magnitude. The localized oscillator strength agrees with the measured radiative lifetime of the exciton, accounting both for its recombining far slower than expected according to the giant oscillator strength and being independent of the NPL area. In the case of the biexciton, on the other hand, theory predicts that the oscillator strength enhancement is determined by the area S_{BX} related to the exciton-exciton interdistance – an internal coordinate – not the area accessible to the biexciton center-of-mass.[20,25] Within that approach, the biexciton oscillator strength f_{BX} ought to be independent of the NPL area by nature, and not diminished by center-of-mass localization.

In this study, we assess this predicted scaling of the oscillator strength f_{BX} of the $\mathrm{X} \rightarrow \mathrm{BX}$ transition by analysing a set of 4.5 ML CdSe NPLs with different areas at room temperature. We first confirm previous findings that exciton absorption and emission are characterized by a total and localized oscillator strength $f_{\mathrm{X},tot}$ and $f_{\mathrm{X},loc}$ respectively, that are related by a fixed, size-independent coherence area. Next, using transient absorption spectroscopy, we

identify the X $\rightarrow$ BX absorption by means of a $\sigma^+\sigma^-$ cross-polarized pump-probe sequence and obtain f_{BX} by spectral integration of the X $\rightarrow$ BX absorption coefficients recorded after creating on average 1 exciton per NPL. Opposite from the total exciton oscillator strength $f_{\mathrm{X},tot}$, we confirm that f_{BX} is independent of the NPL area and agrees with predictions of a short-range interaction model. As shown in literature, the same oscillator strength accounts for stimulated emission across the biexciton-exciton transition. We therefore conclude that, unlike the exciton oscillator strength, f_{BX} is not diminished by center-of-mass localization, a characteristic ensuring that the same oscillator strength is involved in biexciton absorption and stimulated emission. Moreover, our estimate of f_{BX} is comparable to the localized exciton oscillator strength $f_{\mathrm{X},loc}$, a point highlighting the importance of the X $\rightarrow$ BX transition in view of the opto-electronic properties of colloidal NPLs.

As outlined in Figure 2, light absorption by a NPL or quantum well already containing one exciton can result in the formation of a pair of non-interacting excitons or a biexciton or excitonic molecule,*i.e.*, an excitonic complex composed of two interacting excitons. A biexciton can form directly through the optical X $\rightarrow$ BX transition or indirectly by association of two excitons.[14,26,27] The oscillator strength f_{BX} characterizes the direct formation of the biexciton, and is most easily quantified in the case where the biexciton binding energy (Δ_{BX}) is considerably smaller than the exciton binding energy (Δ_X).[20] Under such conditions, f_{BX} can be expressed approximately in terms of the total exciton oscillator strength as:[25]

$$f_{BX} \approx \frac{a_{\mathrm{BX}}^2}{S_{NPL}} f_{\mathrm{X},tot} \approx \frac{S_{BX}}{S_{NPL}} f_{\mathrm{X},tot} \tag{1}$$

Within this approach, f_{BX} provides an order-of-magnitude estimate of the biexciton size and can be seen as a ruler to compare a_{BX} with the relevant exciton extensions, such as the coherence area or the NPL area. In the case of a short range exciton-exciton interaction, a_{BX} can be related to the exciton mass M and the biexciton binding energy Δ_{BX} as $a_{\mathrm{BX}} = \hbar/\sqrt{M\Delta_{\mathrm{BX}}}$;[20] a relation predicting a biexciton radius a_{BX} of 1.2 nm when taking

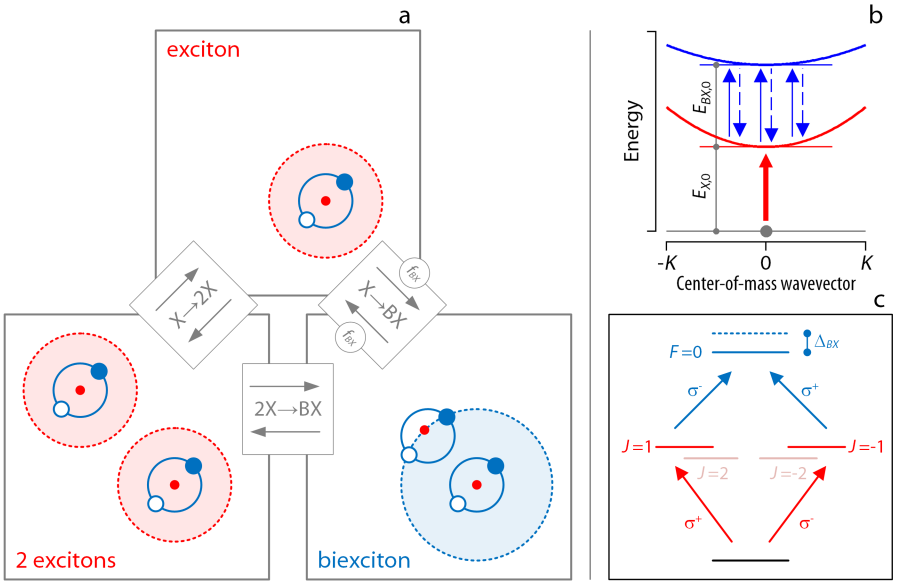

Figure 2: Biexciton formation in CdSe NPLs. (a) The absorption of a photon in the presence of one exciton can lead to the formation of (X $\rightarrow$ BX transition) a biexciton or (X $\rightarrow$ 2X transition) the creation of two separate excitons. Biexcitons can also form through (2X $\rightarrow$ BX transition) the association of two separate excitons, a process governed by thermodynamic equilibrium relations. The reverse biexciton-to-exciton transition can yield net stimulated emission and optical gain. Both biexciton absorption and emission are governed by the oscillator strength f_{BX} of the X $\rightarrow$ BX transition. (b) Band dispersion of the exciton (X) and biexciton (BX) states. The ground state-to-exciton (0 $\rightarrow$ X) and the exciton-to-biexciton (X $\rightarrow$ BX) transitions are indicated by red and blue solid arrows, respectively. The dashed blue arrows indicates stimulated emission along the (BX $\rightarrow$ X) transition. Here $E_{X,0}$ and $E_{BX,0}$ are the exciton and biexciton transition energies at $\mathbf{K} = \mathbf{0}$. (c) Selection rule pathways for the generation of biexcitons in a pump-probe spectroscopy experiment. The creation of a biexciton can proceed only through counter-polarized pump-probe sequences $\sigma^+\sigma^-$ and $\sigma^-\sigma^+$. Δ_{BX} is the biexciton binding energy, while J and F denote the z-component of the exciton or biexciton total angular momentum.

the biexciton binding energy as 50 meV and the exciton mass as the free electron mass. Importantly, given that f_{BX} depends on internal biexciton coordinates only, the biexciton oscillator strength will govern both radiative recombination and stimulated emission through the BX $\rightarrow$ X transition, irrespective of center-of-mass localization, see Figure 2a.

An important difference between exciton and biexciton absorption are the prevailing selection rules, both in terms of conservation of the center-of-mass wavevector $\mathbf{K}$, and the change in total angular momentum upon light absorption. As the NPL ground state has

a zero center-of-mass wavevector, only the formation of the $\mathbf{K} = \mathbf{0}$ exciton is an allowed, bright transition, see Figure 2b. A NPL holding already one exciton, however, can have any center-of-mass wavevector, depending on the state-of-motion of the exciton center-of-mass. In that case, center-of-mass wavevector conservation only restricts the possible X $\rightarrow$ BX transitions to a subset where the biexciton formed has the same center-of-mass wavevector as the exciton initially present. So transitions where $\mathbf{K} \neq \mathbf{0}$ are allowed, as long as $\mathbf{K}$ is conserved. Since the curvature of the center-of-mass dispersion for excitons and biexcitons is different, due to the different quasi-particle effective mass, transitions at different $\mathbf{K}$ will occur at different photon energy and the X $\rightarrow$ BX absorption band will exhibit a broadened tail at lower photon energies. The impact of angular momentum conservation, on the other hand, is best understood starting from the notion that the stable biexciton is typically a singlet with a total angular moment $F = 0$.[28] Hence, disregarding the possibility for spin-flips, the formation of biexcitons through the subsequent absorption of two photons in a pump-probe experiment can be achieved through a cross polarized $\sigma^+\sigma^-$ pulse sequence, but not through co-polarized $\sigma^+\sigma^+$ or $\sigma^-\sigma^-$ sequences, see Figure 2c.[14,29]

We synthesized a set of 4.5 ML CdSe NPLs with increasing area following a modification of the procedure outlined first by Ithurria *et al*,[30] see Supporting Information S1. The analysis of the transmission electron microscopy (TEM) images yielded respective NPLs areas S_{NPL} of 55, 85, 130 and 191 nm^2, see Supporting Information S1. Moreover, ranging from 4.2 to 7.9 nm, the average width of all NPLs exceeds the estimated biexciton radius of 1.2 nm; a point suggesting a negligible impact of lateral confinement on the biexciton properties. Figure 3 represents the linear optical properties relevant to the calculation of the exciton oscillator strength of the 130 nm^2 NPLs as an example. As outlined in Supporting Information S2, similar results are obtained for all other samples included in this study. In particular, Figure 3a shows the spectrum of the intrinsic absorption coefficient $\mu_{i,0}$. In line with literature reports,,[31] we obtained this spectrum by renormalizing the absorbance spectrum at 4.0 eV using the intrinsic absorption coefficient calculated from zinc blende

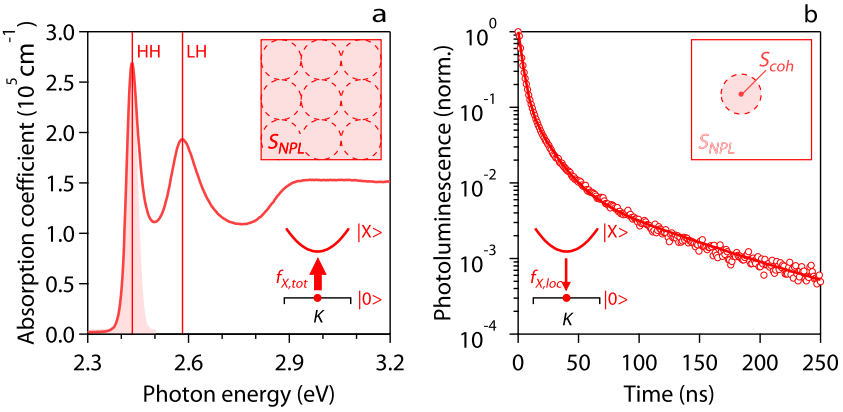

Figure 3: Exciton oscillator strength in CdSe NPLs (a) Intrinsic absorption coefficient spectrum $\mu_{i,0}$. The shaded red region corresponds to the integrated absorption coefficient $\bar{\mu}_{i,0\rightarrow \mathrm{X}}$ which is linked to the *total* exciton oscillator strength $f_{\mathrm{X},tot}$. The inset highlights that this giant oscillator strength is composed of a multitude of parallel transitions forming localized excitons, which preserves the scaling with S_{NPL} irrespective of center-of-mass localization. (b) Photoluminescence intensity decay obtained after excitation at 2.6 eV with a repetition rate of 1 MHz. The red curve corresponds to a triple-exponential fit. The inset indicates that radiative recombination takes place from one of the localized exciton states hosted by the NPLs, such that the rate is related to the localized exciton oscillator strength $f_{\mathrm{X},loc}$ and as such $k_{rad} \propto f_{\mathrm{X},loc} \propto S_{coh}$. The data refer to the NPLs with $S_{NPL} = 130$ nm^2. The results of all the other samples are available in Supporting Information S2.

CdSe bulk optical constants, see Supporting Information S2. The spectrum exhibits the well-known combination of the 2D continuum staircase profile related to free carrier absorption and the pronounced absorption lines reflecting the formation of the heavy-hole (HH) and light-hole (LH) exciton. Decomposing such a spectrum in these contributions (see Supporting Information S2 for details),[11,14,32] we obtained an exciton binding energy Δ_X of about $160-190$ meV; values in line with previous literature reports.[4–7]

The HH absorption feature arises from the ground state-to-exciton transition at $\mathbf{K}=\mathbf{0}$. Since each NPL has one such $0 \rightarrow \mathrm{X}$ transition, the oscillator strength $f_{\mathrm{X},tot}$ can be calculated by integrating $\mu_{i,0}$ across the HH peak, as highlighted in Figure 3a. Specifically, for a nanoplatelet of area S and thickness d dispersed in a solvent with refractive index n_s, the oscillator strength of a generic $\mathrm{A} \rightarrow \mathrm{B}$ transition can be written as:

$$f_{A\rightarrow B} = \frac{2\epsilon_0 n_s m_0 c}{e^2 \pi \hbar^2} \frac{Sd}{|f_{LF}|^2} \bar{\mu}_{i,A\rightarrow B} \tag{2}$$

Here, $\bar{\mu}_{i,\mathrm{A}\rightarrow\mathrm{B}}$ is the energy integrated intrinsic absorption coefficient expressed in $\mathrm{eV}\cdot\mathrm{cm}^{-1}$ and f_{LF} is the local field factor at the energy of the $\mathrm{A} \rightarrow \mathrm{B}$ transition, see Supporting Information S2. Note, for later use, the logic behind Eq 2. The oscillator strength $f_{A\rightarrow B}$ of a *single* transition within a NPL with volume $S \times d$ is obtained by distributing the integrated absorption coefficient $\bar{\mu}_{i,A\rightarrow B}$ over volume elements $S \times d$ large.

As shown in Supporting Information S2, the exciton oscillator strength $f_{\mathrm{X},tot}$ obtained from the integrated absorption coefficient spectrum scales proportionally with the area of the NPLs. As represented in Figure 3a and discussed in literature,[12] this scaling reflects the increasing number of localized exciton states that larger NPLs can host, for which the *total* exciton oscillator strength – interpreted here as the sum over all the localized exciton transitions – matches the oscillator strength of the fully delocalized $\mathbf{K}=\mathbf{0}$ exciton state, see Figure 1a.[9] Radiative recombination, on the other hand, takes places from one of the multiple localized exciton states, see scheme in Figure 3b. As such, the radiative recombination rate

k_{rad} should be related to the localized exciton oscillator strength $f_{\mathrm{X},loc}$ following:[33]

$$k_{rad} = \frac{e^2}{2\pi\epsilon_0 c^3 m_0} n_s |f_{LF}|^2 \omega_{HH} \frac{f_{\mathrm{X},loc}}{2} \tag{3}$$

Here, ω_{HH} is the frequency of the HH transition. As shown in Figure 3b, the PL intensity of the NPLs studied here exhibits a multi-exponential decay, a behavior previously ascribed to a combination of prompt exciton radiative recombination and delayed-emission following a charge-carrier trapping/detrapping sequence.[34,35] We obtained an average luminescence lifetime τ_{avg} for the different samples studied by fitting the PL decay to a triple exponential, and calculate the amplitude-weighted average of the three resulting lifetimes, see Supporting Information S2. This approach yielded an average lifetime ranging from 5.4 to 9.9 ns with increasing NPL area, respectively.

As shown in literature,[12,36,37] an alternative approach to determine the exciton transition dipole moment, and thus the oscillator strength $f_{\mathrm{X},loc}$, makes use of the energy shift of the exciton transition induced by the Optical Stark effect. Such an analysis yielded a transition dipole moment of 18 Debye for 4.5 ML CdSe NPLs of different areas,[12,36] a number translating into $k_{rad} = 0.18\ \mathrm{ns}^{-1}$. Such a rate agrees with the average lifetime of $5.4-6.0$ns obtained here for the largest NPLs; a point confirming that emission is related to radiative recombination from localized excitons.[12,38] The smaller NPLs, however, exhibit a somewhat longer average lifetime of $8.7-9.9$ ns, an increase we assign to the more significant contribution of delayed emission to the average lifetime in these NPLs, see Supporting Information S2. For later reference within this study, we therefore decided to calculate $f_{\mathrm{X},loc}$ for all the investigated samples using a radiative recombination rate $k_{rad} = 0.18\ \mathrm{ns}^{-1}$, rather than the recombination rate obtained from the average lifetime.

Referring to Figure 2c, biexcitons can be formed using a pump-probe sequence with opposite circular polarization. Figure 4 shows the outcome of such an experiment for the 130 nm^2 NPLs. The results of similar experiments on all other investigated samples are

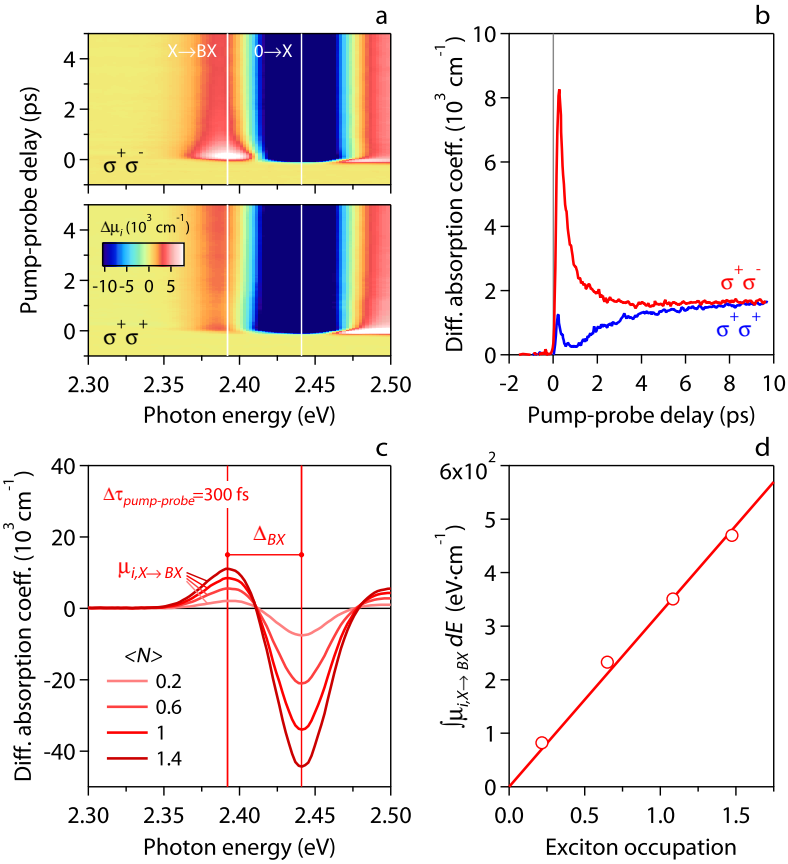

Figure 4: Biexciton spectroscopic signatures in CdSe NPLs. (a) Differential intrinsic absorption $\Delta\mu_i$ map obtained with (top) $\sigma^+\sigma^-$ and (bottom) $\sigma^+\sigma^+$ pump-probe sequences. The sample was excited at the HH exciton transition (2.43 eV) generating an average number of excitons per platelet $\langle N\rangle$=1. (b) Variation of $\Delta\mu_i$ as a function of the pump-probe delay of the X $\rightarrow$ BX transition obtained exciting the sample with (red) $\sigma^+\sigma^-$ and (blue) $\sigma^+\sigma^+$ pump-probe sequences. (c) Counter-polarized $\Delta\mu_i$ spectra at 300 fs for increasing exciton occupation. (d) Energy integrated intrinsic absorption coefficient of the X $\rightarrow$ BX transition for increasing $\langle N\rangle$. The full line is a best fit of the data to a function $\alpha \times \langle N\rangle$, where the fitting parameter α yields the integrated absorption coefficient at $\langle N\rangle$=1. The data refer to the 130 nm^2 NPLs. The results of all the other samples are available in Supporting Information S3.

summarized in Supporting Information S3. In particular, Figure 4a compares the differential intrinsic absorption $\Delta\mu_i$ obtained with $\sigma^+\sigma^-$ and $\sigma^+\sigma^+$ pump-probe sequences for pump excitation resonant to the HH transition (2.43 eV) that creates an average number of exciton $\langle N\rangle$=1 per NPL, see Supporting Information S3. The cross- and co-polarized pump-probe sequences result in strikingly opposite trends. In the $\sigma^+\sigma^-$ map, we observe a pronounced photo-induced absorbance (PA) at the low-energy side of the heavy-hole bleach (2.42 eV) at short pump-probe delays. On the other hand, almost no PA can be discerned with the $\sigma^+\sigma^+$ pump-probe sequence, except for a transient signal at zero delay.

In 2D QWs, Δ_{BX} is expected to be $0.228 \cdot \Delta_X$,[39] a prediction yielding $\Delta_{BX} \approx 45\,\text{meV}$ for the NPLs investigated here. This value agrees well with the difference of 47 meV between the maximum of the red-shifted PA band and the minimum of the HH bleach. Furthermore, the $\Delta\mu_i$ transients follow a peculiar, polarization-dependent behavior, see Figure 4b. The progressive reduction of the $\sigma^+\sigma^-$ signal is mirrored by the in-growth of the $\sigma^+\sigma^+$ intensity, with both signals attaining $\sim$25% of the initial counter-polarized $\Delta\mu_i$ magnitude at longer pump-probe delay. This limiting value can be understood in terms of random scattering across all four available exciton spin states ($J_z = \pm 1, \pm 2$) of which only one yields a bright biexcton transition for a given circular polarization, see Supporting Information S3. Overall, these observations confirm that the PA is the footprint of light absorption across the X $\rightarrow$ BX transition. Hence, we can confidently identify the PA band obtained with counter-polarized pump-probe sequences at short delay-time with the absorption coefficient spectrum of the X $\rightarrow$ BX transition, a quantity we refer to as $\mu_{i,\text{X}\rightarrow\text{BX}}$.

As shown in Figure 4c, the counter-polarized $\Delta\mu_i$ spectrum at 300 fs is characterized by a progressive enhancement of the HH bleach magnitude and the PA intensity for increasing pump fluence. In the case of a diluted exciton gas, the condensations of excitons into biexcitons is rare,[14] and the biexciton absorption line should scale linearly with $\langle N\rangle$ in NPLs of a given size.[25] By integrating the $\Delta\mu_i$ spectra across the PA band, we indeed retrieved this expected linear scaling of $\bar{\mu}_{i,\text{X}\rightarrow\text{BX}}$ with $\langle N\rangle$, see Figure 4d. Moreover, by means of Eq 2,

an integrated absorption coefficient can be recalculated in an oscillator strength, where the oscillator strength f_{BX} of a single X $\rightarrow$ BX transition will be obtained from the integrated absorption coefficient $\bar{\mu}_{i,\mathrm{X}\rightarrow\mathrm{BX}}$ at $\langle N\rangle = 1$; a condition where one X $\rightarrow$ BX transition can occur on average per NPL. We obtained this integrated absorption coefficient as the slope α of the best fit of the function $\alpha\langle N\rangle$ to the $\bar{\mu}_i^{\mathrm{X}\rightarrow\mathrm{BX}}$ *vs.* $\langle N\rangle$ data, see Figure 4d. The same analysis for all the other samples is reported in Supporting Information S3.

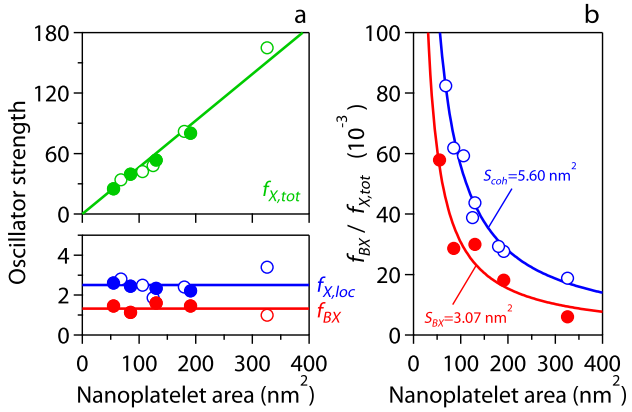

Figure 5: Biexciton oscillator strength in CdSe NPLs. (a) Representation of (green) *total* exciton oscillator strength $f_{\mathrm{X},tot}$, (blue) localized exciton oscillator strength $f_{\mathrm{X},loc}$, and (red) biexciton oscillator f_{BX} as a function of the NPL area. Solid lines are the results of (green, $f_{\mathrm{X},tot}$) linear fits or (blue and red, $f_{\mathrm{X},loc}$ and f_{BX}) represent the average oscillator strength. Full markers pertain to samples included in this study, open marker are taken from literature,[12] or recalculated from literature data.[14] (b) Ratio of (red) the biexciton and the total exciton, and (blue) localized exciton and total exciton oscillator strength as a function of the NPL area. The solid lines are best fits to an $S/\langle N\rangle$ relation, yielding the biexciton and the exciton coherence area as indicated.

Figure 5a represents the total and localized exciton oscillator strength, and the biexciton oscillator strength as obtained from the fit parameter α for all samples investigated here. In addition, the figure contains previously published data obtained on the total and localized oscillator strength,[12] and we recalculated a reported integrated absorption coefficient for the X $\rightarrow$ BX transition in 326 nm^2 4.5 ML NPLs to obtained f_{BX} for that sample in agreement with Eq 2. As can be seen, while $f_{\mathrm{X},tot}$ increases proportionally with S_{NPL}, f_{BX} is largely independent from the NPL area with an average value $f_{BX} = 1.32 \pm 0.13$ over all samples included in Figure 5a. These results confirm the inverse relation between

the oscillator strength ratio $f_{BX}/f_{\mathrm{X},tot}$ and the NPL area S_{NPL} as predicted by Eq 1, and a best fit of $f_{BX}/f_{\mathrm{X},tot}$ to this relation yields an estimate of the biexciton area $S_{BX} = 3.07 \pm 0.23\,\mathrm{nm}^2$. Such a biexciton area agrees reasonably well with the initially estimated biexciton radius of 1.2 nm, which would yield a corresponding area of $\pi a_{BX}^2 = 4.5\,\mathrm{nm}^2$. Clearly, this correspondence highlights the consistency of the analysis put forward in this study, which hinges on the assignment of the X $\rightarrow$ BX in the transient absorption spectrum, and confirms that effects of lateral confinement on the X $\rightarrow$ BX transition are negligible for the NPLs studied here. For completeness, Figure 5c also displays the same analysis for the localized oscillator strength $f_{\mathrm{X},loc}$, from which we obtain the exciton coherence area $S_{coh} = 5.60 \pm 0.12\,\mathrm{nm}^2$ in this case.

According to literature, the same oscillator strength f_{BX} accounts for the material gain obtained through stimulated emission across the BX $\rightarrow$ X transition.[14] Hence, opposite from the exciton where the giant oscillator strength $f_{\mathrm{X},tot}$ still dictates the absorption spectrum while emissive transitions are determined by a diminished localized oscillator strength $f_{\mathrm{X},loc}$, f_{BX} will govern both absorption through the X $\rightarrow$ BX transition and (stimulated) emission across the BX $\rightarrow$ X transition. Accordingly, we conclude that the oscillator strength f_{BX} of the X $\rightarrow$ BX is a quantity independent of the NPL area that is not reduced by exciton localization, a result in line with the notion that f_{BX} is related to internal biexciton coordinates rather than the biexciton center-of-mass coordinate. This area-independence of f_{BX} is one of the factors that underpins the observations that the optical gain characteristics of CdSe NPLs depend on the exciton density, rather than the number of excitons per NPL or the NPL area. Interestingly, Figure 5a and 5b indicate that the oscillator strengths f_{BX} and $f_{\mathrm{X},loc}$ – and thus the biexciton and exciton coherence area – are comparable at room temperature, amounting to 1.32 ± 0.13 and 2.57 ± 0.15, respectively. This finding stresses that light-matter interaction in NPLs through the X $\rightarrow$ BX transition and localized exciton formation or recombination is comparable.

While the short-range interaction model predicts a larger biexciton area for excitons

with a smaller mass, the oscillator strength f_{BX} depends on the product of the biexciton area and the total exciton oscillator strength. This combination involves trade-offs where, for example, a smaller mass enhances the biexciton area but reduces the exciton oscillator strength.[9] Hence, rather than providing rules of thumb to predict f_{BX} in different excitonic materials, the approach introduced here to quantify the X $\rightarrow$ BX transition, and relate the corresponding oscillator strength to the biexciton area, provides a systematic means to rank light-matter interaction through biexciton formation or recombination in different 2D materials by experiments. Such a dataset of experimental biexciton characteristics will complement ongoing theoretical efforts aimed at describing and understanding two-dimensional biexcitons and identify the most promising materials.[28,39,40]

Acknowledgement

Z.H. acknowledges support by FWO-Vlaanderen (research project G0F0920N and medium-scale research infrastructure I004420N). Z.H and I.M acknowledge Ghent University for research funding (BOF-GOA 01G01019). I.M acknowledges the European Research Council (ERC) under the European Union's Horizon 2020 research and innovation program (grant agreement no. 714876 PHOCONA).

Supporting Information Available

Supporting Information is available online and contains information on the synthesis and structural characterization of CdSe nanoplatelets, the photoluminescence decays, the calculation of the intrinsic absorption coefficients and cross sections, circluarly-polarized pump-probe experiments and the calculation of the exciton and biexciton oscillator strengths.

References

(1) Zaslow, B.; Zandler, M. E. Two-Dimensional Analog to the Hydrogen Atom. *Am. J. Phys.* **1967**, *35*, 1118–1119.

(2) Schäfer, W.; Wegener, M. *Semiconductor Optics and Transport Phenomena*; Springer-Verlag: Berlin Heidelberg, 2002.

(3) Mauck, C. M.; Tisdale, W. A. Excitons in 2D Organic–Inorganic Halide Perovskites. *Trends Chem.* **2019**, *1*, 380–393.

(4) Zelewski, S. J.; Nawrot, K. C.; Zak, A.; Gladysiewicz, M.; Nyk, M.; Kudrawiec, R. Exciton Binding Energy of Two-Dimensional Highly Luminescent Colloidal Nanostructures Determined from Combined Optical and Photoacoustic Spectroscopies. *J. Phys. Chem. Lett.* **2019**, *10*, 3459–3464.

(5) Ji, B.; Rabani, E.; Efros, A. L.; Vaxenburg, R.; Ashkenazi, O.; Azulay, D.; Banin, U.; Millo, O. Dielectric Confinement and Excitonic Effects in Two-Dimensional Nanoplatelets. *ACS Nano* **2020**, *14*, 8257–8265.

(6) Kulik, L. V.; Kulakovskii, V. D.; Bayer, M.; Forchel, A.; Gippius, N. A.; Tikhodeev, S. G. Dielectric enhancement of excitons in near-surface quantum wells. *Phys. Rev. B* **1996**, *54*, R2335–R2338.

(7) Shornikova, E. V.; Yakovlev, D. R.; Gippius, N. A.; Qiang, G.; Dubertret, B.; Khan, A. H.; Di Giacomo, A.; Moreels, I.; Bayer, M. Exciton Binding Energy in CdSe Nanoplatelets Measured by One- and Two-Photon Absorption. *Nano Lett.* **2021**, *21*, 10525–10531, PMID: 34874734.

(8) Kumagai, M.; Takagahara, T. Excitonic and nonlinear-optical properties of dielectric quantum-well structures. *Phys. Rev. B* **1989**, *40*, 12359–12381.

(9) Elliott, R. J. Intensity of Optical Absorption by Excitons. *Phys. Rev.* **1957**, *108*, 1384–1389.

(10) 't Hooft, G. W.; van der Poel, W. A. J. A.; Molenkamp, L. W.; Foxon, C. T. Giant oscillator strength of free excitons in GaAs. *Phys. Rev. B* **1987**, *35*, 8281–8284.

(11) Naeem, A.; Masia, F.; Christodoulou, S.; Moreels, I.; Borri, P.; Langbein, W. Giant exciton oscillator strength and radiatively limited dephasing in two-dimensional platelets. *Phys. Rev. B* **2015**, *91*, 121302.

(12) Geiregat, P.; Rodà, C.; Tanghe, I.; Singh, S.; Giacomo, D.; Lebrun, D.; Grimaldi, G.; Maes, J.; Van, D.; Moreels, I. et al. Localization-Limited Exciton Oscillator Strength in Colloidal CdSe Nanoplatelets Revealed by The Optically Induced Stark Effect. *Light Sci. Appl.* **2021**, *10*, 112.

(13) Grim, J. Q.; Christodoulou, S.; Di Stasio, F.; Krahne, R.; Cingolani, R.; Manna, L.; Moreels, I. Continuous-wave biexciton lasing at room temperature using solution-processed quantum wells. *Nat. Nanotech.* **2014**, *9*, 891–895.

(14) Geiregat, P.; Tomar, R.; Chen, K.; Singh, S.; Hodgkiss, J. M.; Hens, Z. Thermodynamic Equilibrium between Excitons and Excitonic Molecules Dictates Optical Gain in Colloidal CdSe Quantum Wells. *J. Phys. Chem. Lett* **2019**, *10*, 3637–3644.

(15) Diroll, B. T.; Talapin, D. V.; Schaller, R. D. Violet-to-Blue Gain and Lasing from Colloidal CdS Nanoplatelets: Low-Threshold Stimulated Emission Despite Low Photoluminescence Quantum Yield. *ACS Photonics* **2017**, *4*, 576–583.

(16) Tomar, R.; Kulkarni, A.; Chen, K.; Singh, S.; Thourhout, D. V.; Hodgkiss, J. M.; Siebbeles, L. D. A.; Hens, Z.; Geiregat, P. Charge Carrier Cooling Bottleneck Opens Up Nonexcitonic Gain Mechanisms in Colloidal CdSe Quantum Wells. *J. Phys. Chem. C* **2019**, *123*, 9640–9650.

(17) She, C.; Fedin, I.; Dolzhnikov, D. S.; Dahlberg, P. D.; Engel, G. S.; Schaller, R. D.; Talapin, D. V. Red, Yellow, Green, and Blue Amplified Spontaneous Emission and Lasing Using Colloidal CdSe Nanoplatelets. *ACS Nano* **2015**, *9*, 9475–9485.

(18) Guzelturk, B.; Pelton, M.; Olutas, M.; Demir, H. V. Giant Modal Gain Coefficients in Colloidal II-VI Nanoplatelets. *Nano Lett.* **2018**, *19*, 277–282.

(19) She, C.; Fedin, I.; Dolzhnikov, D. S.; Demortière, A.; Schaller, R. D.; Pelton, M.; Talapin, D. V. Low-threshold stimulated emission using colloidal quantum wells. *Nano Lett.* **2014**, *14*, 2772–2777.

(20) Golovin, A. A.; Rashba, E. I. Effect of Exciton Interaction on Exciton Spectra. *JETP Lett.* **1973**, *17*, 478–479.

(21) Citrin, D. Long Radiative Lifetimes of Biexcitons in GaAs/$Al_xGa_{1-x}As$ Quantum-Wells. *Phys. Rev. B* **1994**, *50*, 17655–17658.

(22) Ayari, S.; Quick, M. T.; Owschimikow, N.; Christodoulou, S.; Bertrand, G. H. V.; Artemyev, M.; Moreels, I.; Woggon, U.; Jaziri, S.; Achtstein, A. W. Tuning trion binding energy and oscillator strength in a laterally finite 2D system: CdSe nanoplatelets as a model system for trion properties. *Nanoscale* **2020**, *12*, 14448–14458.

(23) Feldmann, J.; Peter, G.; Göbel, E. O.; Dawson, P.; Moore, K.; Foxon, C.; Elliott, R. J. Linewidth Dependence of Radiative Exciton Lifetimes in Quantum Wells. *Phys. Rev. Lett.* **1987**, *59*, 2337–2340.

(24) Efros, A. L.; Wetzel, C.; Worlock, J. M. Effect of a Random Adiabatic Potential on the Optical Properties of Two-Dimensional Excitons. *Phys. Rev. B* **1995**, *52*, 8384–8390.

(25) Combescot, M.; Betbeder-Matibet, O. Biexciton Oscillator Strength. *Phys. Rev. B* **2009**, *80*, 205313.

(26) Kim, J. C.; Wake, D. R.; Wolfe, J. P. Thermodynamics of Biexcitons in a GaAs Quantum Well. *Phys. Rev. B* **1994**, *50*, 15099–15107.

(27) Gourley, P. L.; Wolfe, J. P. Thermodynamics of Excitonic Molecules in Silicon. *Phys. Rev. B* **1979**, *20*, 3319–3327.

(28) Shiau, S.-Y.; Combescot, M.; Chang, Y.-C. Electronic Structure and Absorption Spectrum of Biexciton Obtained by Using Exciton Basis. *Ann. Phys.* **2013**, *336*, 309–330.

(29) Sie, E. J.; Frenzel, A. J.; Lee, Y.-H.; Kong, J.; Gedik, N. Intervalley Biexcitons and Many-Body Effects in Monolayer MoS_2. *Phys. Rev. B* **2015**, *92*, 125417.

(30) Ithurria, S.; Tessier, M. D.; Mahler, B.; Lobo, R. P. S. M.; Dubertret, B.; Efros, A. L. Colloidal Nanoplatelets with Two-Dimensional Electronic Structure. *Nat. Mater.* **2011**, *10*, 936–941.

(31) Achtstein, A. W.; Antanovich, A.; Prudnikau, A.; Scott, R.; Woggon, U.; Artemyev, M. Linear Absorption in CdSe Nanoplates: Thickness and Lateral Size Dependency of the Intrinsic Absorption. *J. Phys. Chem. C* **2015**, *119*, 20156–20161.

(32) Schnabel, R. F.; Zimmermann, R.; Bimberg, D.; Nickel, H.; Lösch, R.; Schlapp, W. Influence of Exciton Localization on Recombination Line Shapes: $In_xGa_{1-x}As$/GaAs Quantum Wells as a Model. *Phys. Rev. B* **1992**, *46*, 9873–9876.

(33) Hens, Z.; Moreels, I. Light Absorption by Colloidal Semiconductor Quantum Dots. *J. Mat. Chem.* **2012**, *22*, 10406–10415.

(34) Rabouw, F. T.; van der Bok, J. C.; Spinicelli, P.; Mahler, B.; Nasilowski, M.; Pedetti, S.; Dubertret, B.; Vanmaekelbergh, D. Temporary Charge Carrier Separation Dominates the Photoluminescence Decay Dynamics of Colloidal CdSe Nanoplatelets. *Nano Lett.* **2016**, *16*, 2047–2053.

(35) Hinterding, S. O.; Salzmann, B. B.; Vonk, S. J.; Vanmaekelbergh, D.; Weckhuysen, B. M.; Hutter, E. M.; Rabouw, F. T. Single Trap States in Single CdSe Nanoplatelets. *ACS Nano* **2021**, *15*, 7216–7225.

(36) Diroll, B. T. Circularly Polarized Optical Stark Effect in CdSe Colloidal Quantum Wells. *Nano Lett.* **2020**, *20*, 7889–7895, PMID: 33118352.

(37) Cunningham, P. D.; Hanbicki, A. T.; Reinecke, T. L.; McCreary, K. M.; Jonker, B. T. Resonant Optical Stark Effect in Monolayer WS_2. *Nat. Comm.* **2019**, *10*, 1–8.

(38) Morgan, D. P.; Kelley, D. F. Exciton Localization and Radiative Lifetimes in CdSe Nanoplatelets. *J. Phys. Chem. C* **2019**, *123*, 18665–18675.

(39) Singh, J.; Birkedal, D.; Lyssenko, V. G.; Hvam, J. M. Binding energy of two-dimensional biexcitons. *Phys. Rev. B* **1996**, *53*, 15909–15913.

(40) Macias-Pinilla, D. F.; Planelles, J.; Climente, J. I. Biexcitons in CdSe Nanoplatelets: Geometry, Binding Energy and Radiative Rate. *Nanoscale* **2022**, *14*, 8493–8500.

Graphical TOC Entry